

Modulation of calcium signaling on demand to decipher the molecular mechanisms of primary aldosteronism

Bakhta Fedlaoui¹, Teresa Cosentino¹, Zeina R. Al Sayed¹, Rita Alexandre Coelho², Isabelle Giscos-Douriez¹, Nicolo Faedda¹, May Fayad¹, Jean-Sebastien Hulot^{1,3}, Chris Magnus⁴, Scott M Sternson⁴, Simon Travers-Allard^{1,5}, Stephanie Baron⁵, David Penton², Fabio L Fernandes-Rosa¹, Maria-Christina Zennaro^{1,6} and Sheerazed Boulkroun^{1#}

¹ Université Paris Cité, Inserm, PARCC, F-75015 Paris France

² Electrophysiology Facility, University of Zurich, Zurich, Switzerland

³ CIC1418 and DMU CARTE, Assistance Publique Hôpitaux de Paris (AP-HP), Hôpital Européen Georges Pompidou, F-75015 Paris, France

⁴ Howard Hughes Medical Institute & Department of Neurosciences, University of California, San Diego, San Diego, United States.

⁵ Service de Physiologie, Assistance Publique Hôpitaux de Paris (AP-HP), Hôpital Européen Georges Pompidou, F-75015 Paris, France

⁶ Service de Génétique, Assistance Publique Hôpitaux de Paris (AP-HP), Hôpital Européen Georges Pompidou, F-75015 Paris, France

#Corresponding author

Address correspondence to:

Sheerazed Boulkroun, PhD

INSERM, U970

Paris Cardiovascular Research Center – PARCC

56, rue Leblanc,

75015 Paris – France

Tel : +33 (0)1 53 98 80 24

Fax : + 33 (0)1 53 98 79 52

e-mail : sheerazed.boulkroun@inserm.fr

Running Title: Molecular mechanisms responsible for PA

Word count – Abstract: 250

Word count – manuscript: 9880

Number of figures: 5

Number of tables: 1

Abstract

Background. Primary aldosteronism is the most common form of secondary hypertension. The most frequent genetic cause of aldosterone producing adenoma (APA) are somatic mutations in the potassium channel KCNJ5. They affect the ion selectivity of the channel, with sodium influx leading to cell membrane depolarization and activation of calcium signalling, the major trigger for aldosterone biosynthesis.

Methods. To investigate how *KCNJ5* mutations lead to the development of APA, we established an adrenocortical cell model in which sodium entry into the cells can be modulated “on demand” using chemogenetic tools (H295R-S2 α 7-5HT3-R cells). We investigated their functional and molecular characteristics with regard to aldosterone biosynthesis and cell proliferation.

Results. A clonal cell line with stable expression of the chimeric α 7-5HT3 receptor in H295R-S2 cells was obtained. Increased sodium entry through the α 7-5HT3 receptor upon stimulation with uPSEM-817 led to cell membrane depolarization, opening of voltage-gated Ca^{2+} channels and increased intracellular Ca^{2+} concentrations, resulting in the stimulation of *CYP11B2* expression and increased aldosterone biosynthesis. Increased intracellular sodium influx did not increase proliferation, but rather induced apoptosis. RNA sequencing and steroidome analyses revealed unique profiles associated with Na^+ entry, with only partial overlap with angiotensin II or potassium induced changes.

Conclusion. H295R-S2 α 7-5HT3-R cells are a new model reproducing the major features of cells harboring *KCNJ5* mutations. Increased expression of *CYP11B2* and stimulation of the mineralocorticoid biosynthesis pathway are associated with a decrease of cell proliferation and an increase of apoptosis, indicating that additional events may be required for the development of APA.

Key words: primary aldosteronism, adrenal cortex, aldosterone biosynthesis, calcium signaling, cell proliferation

Nonstandard abbreviations

ZG: Zona Glomerulosa; PSEM: Pharmacologically Selective Effector Molecules; PSAM: Pharmacologically Selective Actuator Modules; PA: Primary Aldosteronism; APA: Aldosterone Producing Adenoma

Introduction

The adrenal gland consists of two distinct regions: the outer adrenal cortex and the inner adrenal medulla. The adrenal cortex is further divided into three zones: the *zona glomerulosa* (ZG), *zona fasciculata*, and *zona reticularis*, each specialized in hormone production due to the expression of specific enzymes. Among these hormones, aldosterone, produced by the adrenal ZG, plays an important role in regulating salt and fluid balance, thereby controlling arterial blood pressure. As a key component of the renin-angiotensin-aldosterone system (RAAS), its production is mainly stimulated by angiotensin II (AngII), which increases in response to volume depletion, and elevated plasma potassium (K^+) levels^{1,2}. AngII signals through its type 1 receptor (AT1R) and activates, via G_{aq}, an entire signaling cascades that leads to the release of Ca^{2+} from the endoplasmic reticulum. The stimulation by K^+ and to a less extend by AngII results in ZG cell membrane depolarization and opening of voltage-gated calcium (Ca^{2+}) channels, leading to an increased intracellular Ca^{2+} concentration. The activation of Ca^{2+} signaling triggers a phosphorylation cascade that leads to increased transcription of *CYP11B2*, coding for aldosterone synthase, and aldosterone biosynthesis¹.

Deregulation of the mechanisms regulating adrenal aldosterone biosynthesis results in primary aldosteronism (PA). PA is the leading cause of secondary hypertension affecting approximately 5-10% of hypertensive patients and up to 20% of those with treatment resistant hypertension³⁻⁶. It is characterized by hypertension with elevated aldosterone levels, low plasma renin concentration, increased aldosterone to renin ratio and often associated with hypokalaemia. The main subtypes of PA are bilateral adrenal hyperplasia and aldosterone-producing adenomas (APA), accounting together for 95% of cases. PA is associated with an increased risk of cardiometabolic and renal complications⁷ due to the major adverse effects of aldosterone excess; therefore, early diagnosis and appropriate treatment of PA are essential.

In the past decade, research has uncovered mutations in ion channels (*KCNJ5*⁸, *CACNA1D*^{9,10}, *CACNA1H*^{11,12}, *CLCN2*^{13,14}, *SLC30A1*¹⁵) and pumps (*ATP1A1*^{9,16}, *ATP2B3*¹⁶), as principal causes of APA and familial forms of PA. These mutations enhance either directly or indirectly intracellular Ca²⁺ concentrations, the main trigger for aldosterone biosynthesis. Notably, in the case of *KCNJ5*, which encodes the G protein-coupled inwardly rectifying K⁺ channel (GIRK4), the majority of mutations cluster near the channel's ion-selective filter, leading to a loss of selectivity for K⁺ ions in favour of an intracellular sodium (Na⁺) influx⁸. These mutations lead to cell membrane depolarization, the opening of voltage-gated Ca²⁺ channels, an increase of intracellular Ca²⁺ concentration, activation of Ca²⁺ signalling pathways, and ultimately an increase of *CYP11B2* expression and aldosterone biosynthesis⁸.

While the role of *KCNJ5* mutations in autonomous aldosterone production has been well established, their role in modulating cell proliferation is still under debate^{17–20}. The first objective of our study was therefore to investigate the role of *KCNJ5* mutations in regulating proliferative processes that could lead to adenoma development. The second objective was to determine whether changes in intracellular sodium balance could induce specific intracellular transcriptional profiles that could explain the peculiar pathological and biological features of adenoma carrying *KCNJ5* mutations. For this purpose, we used chemogenetic tools which allow to manipulate specific ion fluxes via modified ion channels with pharmacologically selective properties, known as Pharmacologically Selective Actuator Modules (PSAM). PSAM, comprising mutated ligand-binding domains and selective ionic pore domains respond to Pharmacologically Selective Effector Molecules (PSEM), inducing channel opening and allowing specific ions to flow through the activated channel^{21,22}. Here we employed second-generation chemogenetic tools to establish a human adrenal cell model in which we could modulate sodium entry on demand, by introducing the α7-5HT3 chimeric receptor. This chimeric receptor consists of the ligand binding domain of the α7 nicotinic acetylcholine

receptor and the ionic pore domain of the serotonin receptor type 3. Importantly, the ligand binding domain has been mutated to bind only the PSEM and not the endogenous ligand²¹. Activation of this α 7-5HT3 receptor (α 7-5HT3-R) by uPSEM-817 was used to study the effect of Na⁺ entry into the cells, mimicking molecular abnormalities observed in the presence of *KCNJ5* mutations. To determine the functional and molecular characteristics of this new cell model, we assessed changes in membrane potential, intracellular Ca²⁺ concentration, and impact on cell proliferation. Additionally, we conducted RNA sequencing and steroidomic analyses following treatment with uPSEM-817, AngII, and K⁺.

Material and Methods

Data Availability

An expended Methods section is available in the online-only Data Supplement.

The data, analytic methods and study materials that support the findings of this study are available from the corresponding author upon reasonable request.

Cell culture and electroporation

The H295R-S2 cell line, a subclone of the H295R human adrenocortical carcinoma cell, was kindly provided by Dr. William E. Rainey²³ and cultured in complete medium containing DMEM/Eagle's F12 medium (1:1) (GIBCO, Life Technologies) supplemented with 2% Ultroser G (Sartorius, France), 1% insulin/transferrin/selenium premix (BD Bioscineces), 7.5 mM HEPES (GIBCO), 1% penicillin and streptomycin (GIBCO, Life Technologies) and 20 mg/mL G418 (Thermo Fisher Scientific). Cells were maintained at 37°C under a humid atmosphere of 95% air and 5% CO₂.

The α7-5HT3 chimeric receptor consists of the ligand binding domain of the nicotinic receptor fused with the ionic pore domain of the serotonin receptor type 3. The sequence has been inserted into pcDNA3.1 vector²¹.

5.000.000 of H295R-S2 cells were seeded into a 100mm tissue culture dish. After 24h cells were trypsinized, counted and 3.10⁶ cells resuspended in 100μl Nucleofactor R solution and electroporated with 3μg of plasmid (pcDNA3 containing or not α7-5HT3 cDNA) using the Amaxa nucleofactor kit R (Lonza) according to the manufacturer instructions. After electroporation, the mixed populations were amplified in under selection pressure with G418. Pure clones were isolated by picking clones after limited dilution of the cells in order to isolate

one cell at an optimum distance from the other in a 200mm diameter plate. Colonies were, afterwards, isolated in wells and amplified for further characterization.

Statistics

The number of independent experiments (n) refer to the number of cells or dishes studied to calculate mean \pm SEM or medians. The measurements were carried out at different days and from different cell preparations using different cell passages to ensure the reproducibility of the experiments. For patch-clamp experiments, each cell was analyzed separately.

Data were analysed in Prism10 software (GraphPad, San Diego, CA) using the appropriate statistical tests as indicated in the text. The normality of the data distribution was checked using the ShapiroWilk test. Quantitative variables were reported as means \pm s.e.m. when a Gaussian distribution was present or as medians and interquartile ranges when no Gaussian distribution was present. Pairwise comparisons were conducted using unpaired t tests for normally distributed data and Mann–Whitney tests for non-normally distributed data. For multiple comparisons, ANOVA followed by Bonferroni was applied when data presented a Gaussian distribution while Kruskal–Wallis followed by Dunn’s test was used for non-Gaussian distribution was present. A *p* value < 0.05 was considered significant.

Results

Characterization of a cell model expressing the α7-5HT3 receptor

To assess the impact of modulating intracellular Na⁺ concentration on adrenal cell function, we established stable expression of the chimeric α7-5HT3-R in H295R-S2 cells. This receptor was formed by combining the extracellular ligand-binding domain of the α7 nicotinic acetylcholine receptor and the ion pore domain of the serotonin receptor 5HT3²¹. Expression of the α7-5HT3-R was investigated by RT-qPCR²⁴ and found exclusively in cells transfected with the vector containing its genetic sequence (Figure S1A), but not in control cells transfected with an empty vector. Upon treatment with 12mM of K⁺ both cell lines exhibited a rapid increase in intracellular Ca²⁺ concentration (Figure S1B). However, treatment with different concentrations of varenicline, a nicotinic receptor partial agonist and cholinergic agonist, resulted in a dose-dependent increase in intracellular Ca²⁺ concentration in cells expressing the α7-5HT3-R only (Figure S1B), indicating a specific effect on the chimeric receptor. This was associated with an increase in *CYP11B2* mRNA expression for varenicline concentrations ranging from 10⁻⁸ to 10⁻⁵M (Figure S1C).

To further characterize the cells expressing the α7-5HT3-R, monoclonal cell populations were obtained via limiting dilution under antibiotic selection pressure. Among the 19 monoclonal cell populations selected, six showed α7-5HT3-R mRNA expression (Figure S1D), and in-depth characterization was carried out on three of them, designated as clones 17, 24, and 42 (Figure 1). The expression of α7-5HT3-R mRNA was not statistically different between clones 17, 24, and 42 (Figure 1A).

Brightfield images revealed no discernible variations in cell morphology between control cells and the three selected clones (Figure 1B). Examination of the cellular localization

of the α 7-5HT3-R using α -bungarotoxin, a peptide binding to the α subunit of the nicotinic acetylcholine receptor, showed its presence on the cell surface of clones 17, 24, and 42 but not in control cells (Figure 1B). To ensure that the expression of the α 7-5HT3-R did not induce structural changes, we studied the expression of markers of cytoskeletal organisation and of ZG cells. Phalloidin staining revealed similar actin organization in cells expressing an empty vector (control cells) or expressing the α 7-5HT3-R (Figure 1B). A similar staining was observed for Disabled-2 (Dab2) (Figure 1B), a protein marker of ZG cells expressed at the cell membrane.

Varenicline is a nicotinic receptor partial agonist and a cholinergic agonist, which may have non-specific effects in our cell model. To avoid this, we compared the effect of varenicline to those of a drug, uPSEM-817, specifically designed to bind to the α 7-5HT3-R. Similar responses were obtained in response to uPSEM-817 and varenicline treatment in intracellular Ca^{2+} responses, both as traces (Figure S2A, S2C) and maximum of activation (Figure S2B, S2D).

α 7-5HT3 receptor activation by PSEM-817 induces cell membrane depolarization and increases intracellular Ca^{2+} content via Na^+ influx

Perforated patch-clamp recordings were conducted to assess the electrophysiological properties of two of the three clones expressing the α 7-5HT3-R and selected for further investigations (clones 17 and 42) in comparison to control cells. Control cells expressing an empty vector, as well as clones 17 and 42, displayed similar membrane hyperpolarization with membrane potentials of -60.83 ± 1.2 , -61.73 ± 1.16 , and -63.27 ± 1.26 , respectively (Figure 2A), indicating that the α 7-5HT3-R was not leaking ions.

All the clones responded to induction by AngII, exhibiting membrane depolarization upon the application of 10^{-8}M AngII ($\Delta E_m = 48.26 \pm 3.52$, 51.81 ± 3.73 , 46.00 ± 3.51 for control

cells, clones 17 and 42 respectively) (Figure 2B). However, only clones 17 and 42 were responsive to 10^{-7} M ($\Delta Em=41.58\pm4.12$ and 41.49 ± 2.13 for clones 17 and 42 respectively) and 10^{-5} M of uPSEM-817 ($\Delta Em=49.03\pm5.51$ and 47.19 ± 2.24 for clones 17 and 42 respectively). The lower concentration of 10^{-9} M uPSEM-817 did not consistently induce membrane depolarization (Figure 2B).

Electrophysiological measurements were performed using High Throughput Automated Patch-Clamp to determine whether activation of the $\alpha 7$ -5HT3-R by uPSEM-817 increased Na^+ current. Repetitive stimulations using a voltage ramp from -100mV to +20mV that was used to calculate the reversal potential (E_{Rev}) (Figure S3A), a surrogate of the resting membrane voltage, confirmed that uPSEM-817 induced depolarization of clones 24 and 42 compared to vehicle treated cells (Figure S3B). Inward currents were measured at -100mV as they correspond to positive charges (e.g. Na^+ ions) entering the cells. Treatment with 10^{-6} M of uPSEM-817 under extracellular Na^+ concentrations of 80mM or 132.5mM activated a statistically significant inward current in clone 42 and a similar trend in clone 24 (Figure S3C). These results are consistent with an increase of Na^+ permeability when cells were treated with uPSEM-817.

To determine whether the membrane depolarization triggered by uPSEM-817 correlated with an increase in intracellular Ca^{2+} concentration, $\alpha 7$ -5HT3-R expressing cells were exposed to concentrations of uPSEM-817 ranging from 10^{-9} to 10^{-5} M, as well as 12mM K^+ and 10^{-8} M AngII as positive controls (Figure 2C-E). The results are presented for clone 17 (Figure 2C-E) and similar results were obtained for clone 42 (Figure S4). Application of AngII or K^+ led to a rapid increase in intracellular Ca^{2+} levels followed by a rapid decline without returning to baseline levels (Figure 2C, Figure S4A), occurring after similar response latency (data not shown). The maximum of activation (Figure 2D, Figure S4B) was significantly increased when

cells were treated with AngII or K⁺. The area under the curve (AUC) at the peak (between 0 and 360s) (Figure 2E, left panel, Figure S4C) and at the steady state response (between 0 and 700s) (Figure 2E, right panel, Figure S4D) were also significantly increased after K⁺ or AngII treatment, these increases being more important when cells were treated with K⁺. Treatment with uPSEM-817 ranging from 10⁻⁹ to 10⁻⁵M also resulted in a similar rapid increase in intracellular Ca²⁺ content; this increase was more modest at 10⁻⁹M uPSEM-817 compared to higher concentrations of the compound. Interestingly, the decline following the peak was slower with uPSEM-817 compared to AngII or K⁺ (Figure 2C, Figure S4A). Maximum activation (Figure 2D, Figure S4B) and AUC at the peak (Figure 2E, left panel, Figure S4C) and at steady state (Figure 2E, right panel, Figure S4D) were lower in response to 10⁻⁹M of uPSEM-817 than with 10⁻⁷ and 10⁻⁵M uPSEM-817. Despite variations in Ca²⁺ content, while the maximum activations were comparable when cells were treated with AngII, K⁺, 10⁻⁷ and 10⁻⁵M uPSEM-817, the AUC at the steady state were significantly higher when cells were treated with 10⁻⁷ and 10⁻⁵M uPSEM-817 compared to AngII and K⁺. The sustained higher Ca²⁺ content when cells were treated with PSEM suggests the activation of different mechanisms compared to AngII and K⁺.

α7-5HT3 receptor activation by uPSEM-817 activates steroidogenesis

The steroidome of clones 17, 24 and 42 was determined using the cell supernatant after 8h (Figure S5A-B) or 24h (Figure S5C-D) of treatment with 10⁻⁸M AngII or 12mM K⁺ as positive controls (Figure S5A, S5C), and uPSEM-817 ranging from 10⁻⁹ to 10⁻⁵M (Figure S5B, S5D), and the results presented separately for each clone (Figure S5). Interestingly, despite similar modification in intracellular Ca²⁺ concentration, different profiles were obtained for the three different clones in response to AngII, K⁺ and uPSEM-817. However, they converge all towards a stimulation of steroid biosynthesis in response to uPSEM-817. Among the 19 steroids

measured, only 14 were detectable after 8h and 24h of treatment. After 8h of treatment, an overall activation of steroid biosynthesis was observed in response to AngII and K⁺ (Figure S5A, Table 1). Similarly, uPSEM-817 at concentrations from 10⁻⁷ to 10⁻⁵M led to an increase in steroid biosynthesis, with no significant changes observed at 10⁻⁹ and 10⁻⁸M of uPSEM-817 (Figure S5B, Table 1). Interestingly, the increases in certain steroids due to uPSEM-817 were less pronounced compared to those induced by AngII and K⁺. After 24h of treatment, a significant decrease in the concentration of two steroid precursors, pregnenolone and progesterone, was observed in response to AngII and K⁺, while DOC, 17-hydroxyprogesterone, 17-hydroxypregnenolone, pregnenolone and progesterone concentrations remained elevated in response to uPSEM-817 (Table 1). Aldosterone biosynthesis was highly stimulated by AngII and K⁺ and to a lesser extent by uPSEM-817. While no effect was observed after 8h of treatment, after 24h the concentration of 18-oxocortisol was significantly increased in response to K⁺, and a trend was also observed in response to AngII and for all the concentrations of uPSEM-817. The concentrations of 18-hydroxcortisol were undetectable in all tested conditions.

T-type and L-type channels are both involved in Ca²⁺ entry into the cells in response to uPSEM-817

Both T-type and L-type voltage-gated Ca²⁺ channels have been shown to be involved in aldosterone biosynthesis regulation by modulating intracellular Ca²⁺ concentrations^{25,26}. We evaluated the effect of a 2h pre-treatment with 10⁻⁶M of the L-type Ca²⁺ channel blocker nifedipine, or 10⁻⁶M of the T-type Ca²⁺ channel blocker mibepradil on the modulation of intracellular Ca²⁺ content in response to 10⁻⁸M AngII, 12mM K⁺ and increasing concentrations of uPSEM-817 (Figure 3A-C). Interestingly, pre-treatment of the cells with nifedipine or mibepradil partially abolished Ca²⁺ entry into the cells after treatment with K⁺ and uPSEM-817,

as revealed by lower peak (Figure 3A-B) and decreased AUC (representing the modifications of intracellular Ca^{2+} concentrations, illustrating activation of Ca^{2+} signaling) (Figure 3C). In contrast, nifedipine and mibepradil had no effect on the initial entry of Ca^{2+} into the cell in response to AngII (Figure 3B), and only nifedipine pre-treatment led to a significant decrease in the AUC (Figure 3A-C). These results indicate that both T- and L-type Ca^{2+} channels are mobilized to allow Ca^{2+} entry into the cells in response to K^+ and uPSEM-817, a mobilization that appears to be greater than in response to AngII.

To determine if the differences observed in the modulation of intracellular Ca^{2+} concentration in response to Ca^{2+} channel blockers and uPSEM-817 cotreatment were due to differences in cell membrane depolarization, we performed patch-clamp analyses (Figure 3D). Prior to the administration of 10^{-7}M uPSEM-817, we treated each patched cell with 10^{-6}M mibepradil, or with 10^{-6}M Nifedipine. These blockers were applied locally using an ejector solution. The results displayed a range of responses among cells: in certain instances, the blockers effectively suppressed depolarization, returning the membrane potential to a state near its baseline ($\Delta\text{EM} \approx 0$); while in other cases, the membrane remained depolarized, albeit to a lesser degree than when exposed exclusively to 10^{-7}M uPSEM-817 (Figure 3D).

$\alpha 7$ -5HT3 receptor activation by uPSEM-817 led to a decrease in cell proliferation and an increase of apoptosis

To evaluate the impact of elevated intracellular Ca^{2+} concentration on cell proliferation, cells were treated with 12mM K^+ or 10^{-9} to 10^{-5}M uPSEM-817 for 24h and 72h. The number of viable proliferating cells was determined using a colorimetric method. Whereas following 24h of treatment, cell proliferation remained unaffected by K^+ or uPSEM-817 treatment, a decrease in cell proliferation was observed after 72h of treatment with the higher concentration of uPSEM-817 (Figure 4A).

To explore the impact on cell cycle progression of AngII, K⁺ and uPSEM-817 treatment, we assessed the cell cycle phase distribution using propidium iodide staining and cytometric analysis at 8h, 24h, 48h, and 72h. Treatment with AngII for 8h resulted in a reduction in the percentage of cells in the G1 phase and an increase in the percentage of cells in G2 compared to untreated cells suggesting an increase in cell proliferation (Figure 4B). After 24h of AngII treatment, an increase in the percentage of cells in the G1 phase and a decrease in the S phase was also observed. Longer exposure to AngII had no effect on the distribution of cells across different phases of the cell cycle. In response to K⁺ treatment, a similar pattern was observed with a decrease in the percentage of cells in G1, and an increase in G2 after 8h. While no alterations in cell distribution were noted after 24h of K⁺ treatment, an increase in the percentage of cells in G1 and a decrease in G2 was observed (Figure 4B). Conversely, treatment with uPSEM-817 did not affect cell distribution among the different phases compared to untreated cells (Figure 4C). We assessed the effect of uPSEM-817 on apoptosis by determining the proportion of cells in the sub-G1 phase. The sub-G1 phase reflects DNA fragmentation which occurs in the late stage of apoptosis. Similar to what was observed for cell proliferation results, no effect was observed when cells were treated with uPSEM-817, AngII and K⁺ for 24h (Figure 4D). At 72h, a significant increase in the percentage of cells in sub-G1 phase was observed in response to K⁺, AngII and uPSEM-817 (10⁻⁷M) (Figure 4E), indicating an increase in cell apoptosis.

α7-5HT3 receptor activation by uPSEM-817 results in the activation of specific pathways

To gain insight into the impact of modulating intracellular Na⁺ concentration in cells expressing the α7-5HT3-R, we conducted RNA sequencing analysis on these cells (clones 17, 24, and 42) following treatment with 10⁻⁷M uPSEM-817 for 8h (Figure S6 and S7) and 24h (Figure 5, S8). Hierarchical clustering effectively segregated cells treated for 8h and 24h from

untreated cells (Figure S6A, S7A, S8A, 5A). After 8h of treatment, we identified 28 differentially expressed genes with a fold change of at least 0.5; 18 upregulated genes (64.29%) and 10 downregulated genes (35.71%) (Table S2). Gene ontology analyses unveiled 18 specific enriched biological processes in uPSEM-817 treated cells (Figure S6B, Table S3), primarily related to Ca^{2+} ion transport and signalling pathways, cell adhesion, and aldosterone synthesis and secretion. Following 24h of treatment, 30 genes were differentially expressed with a fold change of at least 0.5, with 22 genes (73.33%) upregulated and 8 (26.67%) downregulated (Figure 5B, Table S4)^{27,28}. Enriched pathways included protein regulation of GTPase activity, Ras protein signal transduction, and aldosterone synthesis and regulation (Figure 5B, Table 3). These analyses were completed by using Gene Set Enrichment Analysis (GSEA) and Hallmark database that provides information on most universal cellular mechanisms (Figures S7, S8). Using an FDR <25% we identified 6 differentially regulated pathways after 8h of treatment with PSEM and 7 after 24h. After 8h of treatment, TNF α signaling via NF κ B and coagulation pathway were found enriched in basal condition (Figure S7B) whereas Kras signaling, heme metabolism, UV response and Interferon alpha response were found to be enriched in response to uPSEM-817 (Figure S7C). After 24h of treatment (Figure S8), only TNF α signaling via NF κ B pathway (Figure S8B) was enriched in basal condition and Myc targets, oxidative phosphorylation, DNA repair Apical surface, unfolded protein response and G2M checkpoint pathways were enriched after uPSEM-817 treatment (Figure S8C).

To identify genes and pathways specifically regulated by modulation of intracellular Na^+ concentration, we also performed RNA sequencing on $\alpha 7\text{-5HT3-R}$ expressing cells treated with 12mM K^+ and 10^{-8}M AngII for 8h and 24h (Figure S6, S9, Figure 5). After 8h of treatment, 4932 genes were differentially expressed in response to AngII and 728 in response to K^+ (Figure S6C, S6G, Table S6, Table S7). Gene ontology analyses^{27,28} for 8h AngII treatment revealed enrichment in 390 different pathways (Table S8), with significant involvement in the regulation

of reticulum activity, negative regulation of cell growth, and aldosterone, cortisol and parathyroid hormone synthesis and secretion (Figure S6D). Eight hours of treatment with K⁺ resulted in enrichment of 211 pathways (Table S9), including membrane depolarization during action potential, Ca²⁺ and Na⁺ ion transport, and circadian rhythm (Figure S6H). Interestingly, both AngII and K⁺ treatment led to enrichment in positive regulation of transcription and MAPK signaling pathways. Among the 28 differentially expressed genes in response to uPSEM-817, 17 were common to AngII (*OLFML2B*, *RGPD6*, *LMOD1*, *MAT1A*, *MC2R*, *CA2*, *CACNA1C*, *EGFR*, *ETV5*, *TNXB*, *PFKP*, antisense to *WASF3*, antisense to *ERVW-1* and *PEX1*, *PPP2R1B*, *LYPLAL1-AS1*, *LONRF2* and *ST6GALNAC6*) (Figure S6E) and 12 to K⁺ (*OLFML2B*, *LMOD1*, *MAT1A*, *MC2R*, *CA2*, *CACNA1C*, *ATP8B4*, *ETV5* *PFKP*, *PPP2R1B*, *LYPLAL1-AS1* and *LONRF2* (Figure S6I). Among the 18 enriched pathways in response to uPSEM-817, 9 were commonly enriched in response to AngII (Figure S6F) and 5 in response to K⁺ (Figure S6J). Most importantly, 11 genes were specifically regulated by uPSEM-817 when compared with AngII (*HPX*, *EPHA10*, *ATP8B4*, *HHIP*, *MICAL1*, *RBMS2*, *E9PAM4*, *H7C2Y5*, *TP53TG3B*, *DUXAP8* and *RNVU1-7*) and 16 when compared to K⁺ (*HPX*, antisense to *WASF3*, *EPHA10*, *HHIP*, *ST6GALNAC6*, antisense to *ERVW-1* and *PEX1*, *EGFR*, *MICAL1*, *TNXB*, *RGPD6*, *RBMS2*, *E9PAM4*, *H7C2Y5*, *TP53TG3B*, *DUXAP8* and *RNVU1-7*). This allowed us to define a specific Na⁺-induced specific signature composed of 10 genes (*HPX*, *EPHA10*, *HHIP*, *MICAL1*, *RBMS2*, *E9PAM4*, *H7C2Y5*, *TP53TG3B*, *DUXAP8* and *RNVU1-7*) (Figure S10).

After 24h of treatment, 589 genes were statistically differentially expressed in response to AngII (Figure 5C, 5D, Table S10). Among them, 12 were common to uPSEM-817 (*SOBP*, *ADRA2A*, *ETV5*, antisense to *DLGAP1*, *VSIR*, *GCNA*, *FCHSD1*, *RAPGEFL1*, *PPP2R1B*, *CYP11B2*, *LYPLAL1-AS1* and *PRSS53*); 146 pathways were specifically enriched in response to AngII and 2 (Cushing syndrome and Aldosterone synthesis and secretion) were commonly

enriched in response to AngII and uPSEM-817 (Figure S9B, Table S11). Interestingly, enriched pathways included those associated with cell adhesion and extracellular matrix organization (Figure S9A). K⁺ treatment for 24h led to the regulation of 798 genes (Figure S7A, 5F, Table S12), among them 12 were common to uPSEM-817 (*KLF10*, *ADRA2A*, *C9ORF72*, *MC2R*, *ETV5*, *RAPGEF4*, *VSIR*, *GCNA*, *FCHSD1*, *PPP2R1B*, *CYP11B2* and *LYPLAL1-AS1*). Similarly, enriched pathways included those associated with cell adhesion and extracellular matrix organization (Figure S9C, Table S13). Five out of the eight enriched pathways identified in response to uPSEM-817 treatment were also commonly enriched in response to K⁺ (Figure S9D). These common pathways involved positive regulation of GTPase activity, Cushing Syndrome, Negative regulation of cell migration, Ras protein signal transduction, and Aldosterone synthesis and secretion. Notably, Cushing syndrome and aldosterone biosynthesis and secretion pathways were also commonly enriched between uPSEM-817 and AngII. We were able to define a 24h sodium-specific signature composed by 14 genes (*FMNL1-AS1*, *IDI2-AS1*, *WHAMMP1*, *MUSTN1-ITIH4 Readthrough*, *NFKBIZ*, *KCNQ1OT1*, *SH3BP5-AS1*, *CDK10*, *PTPRU*, *IL17RD*, *TMEM67*, *MAZ-AS*, *DOPIB* and one unknown sequence) (Figure S11).

The list of differentially expressed genes was compared to their expression in 11 control adrenal and 123 APA retrieved from transcriptomic data²⁹ (Table S14, S15). Of these 123 APA, 50 carried a mutation in the *KCNJ5* gene and 73 in another APA driver gene; the comparison was therefore made between the 11 control adrenals, the 50 APA with a mutation in the *KCNJ5* gene and the 73 APA without a mutation in the *KCNJ5* gene. After 8h of treatment with 10⁻⁷M of uPSEM-817, among the 55 identified genes that were significantly differentially expressed without consideration of the fold change, the expression of 49 were found in our transcriptomic data from control adrenals and APA and could be retrieved. In these data, no expression was detected for five genes, and out of the remaining 44 genes, 13 were also found to be

differentially expressed in APA compared to control adrenal (Table S12), two only in APA with a KCNJ5 mutation (*HPX* and *WHRN*) and three in APA without KCNJ5 mutation (*ETV5*, *GPAM* and *OLFML2B*). Interestingly, among the 13 genes differentially expressed in APA independently of the mutational status, 4 were found to be up-regulated (*CACNA1C*, *ATP2B2*, *VDR* and *EPHA10*) and 1 downregulated (*RGPD6*) in both APA and α 7-5HT3-R cells, whereas 6 genes were found to be upregulated in α 7-5HT3-R cells but downregulated in APA (*PPP2R1B*, *LONRF2*, *ATP8B4*, *TNXB*, *ITGA7* and *HSPA12A*), independently of the mutational status and 2 down-regulated in response to uPSEM-817 but up-regulated in all APA (*TMEM200A* and *ELL2*). Similarly, after 24h of treatment, among the 73 genes identified genes that were significantly differentially expressed regardless of the fold change, the expression of 64 genes could be retrieved from our transcriptomic data. No expression was found for 10 genes, and among the remaining 54 genes, 15 were also found to be differentially expressed in APA compared to control adrenal (Table S13). Among these 15 genes, three were found to be commonly upregulated in both α 7-5HT3-R cells and APA (*FCHSD1*, *CACNA1C* and *TTNI*) and one downregulated (*KLF10*) whereas two were found to upregulated in α 7-5HT3-R cells and downregulated in APA, independently of the mutational status (*PPP2R1B* and *NEAT1*) and four downregulated in α 7-5HT3-R cells and upregulated in all APA (*STMN3*, *FIBCD1*, *FSCN1* and *CCDC71L*). Interestingly, three genes were found to be significantly regulated only in APA without KCNJ5 mutations, two downregulated in α 7-5HT3-R cells but upregulated in APA (*ETV5* and *CEP170*) and one downregulated in both (*NR2F2*); two genes were found to be significantly regulated only in APA with KCNJ5 mutations, one downregulated in α 7-5HT3-R cells but upregulated in APA (*NFKBI2*) and one downregulated in both (*ABHD2*). Interestingly, none of the genes commonly regulated in α 7-5HT3-R cells and APA belongs to the Na^+ signature defined after 8h and 24h of treatment suggesting that they are probably involved in the early phase of APA development.

Discussion

Somatic *KCNJ5* mutations are the most frequent genetic abnormalities found in APA with a prevalence between 43% and 75% of cases. APA with *KCNJ5* mutations are more frequent in women and at younger age^{29,30} and are characterized by hybrid steroid production and larger adenoma size³¹. Expression of mutated *KCNJ5* in adrenocortical cells leads to increased aldosterone production without increasing cell proliferation^{17,19}, raising the question as to whether those mutations are sufficient to lead to both increased aldosterone production and adenoma formation. Here we describe the development of an adrenocortical cell model that recapitulates the main features of *KCNJ5* mutations, by modulating “on demand” sodium entry into the cells using chemogenetic tools. Increased sodium entry through the chimeric $\alpha 7\text{-}5\text{HT3}$ -R upon stimulation with uPSEM-817 led to cell membrane depolarization, opening of voltage-gated Ca^{2+} channels and increased intracellular Ca^{2+} concentrations, resulting in the stimulation of *CYP11B2* expression and increased aldosterone biosynthesis.

The steroid response of H295R-S2 $\alpha 7\text{-}5\text{HT3}$ -R cells to AngII is similar to that described in H295R cells³², with an early and transitory increase of pregnenolone, progesterone and 11-deoxycorticosterone and a late and sustained production of aldosterone and corticosterone³². In contrast, sodium entry into the cells induced by uPSEM-817 led to a specific steroid profile only partially overlapping with that induced by AngII and K^+ . In particular, we observed a prolonged induction of early steroid precursors and DOC, suggesting an action on both early and late steps of aldosterone biosynthesis, as well as a delayed and smaller induction of aldosterone biosynthesis; there was no induction of glucocorticoid biosynthesis in H295R-S2 $\alpha 7\text{-}5\text{HT3}$ -R cells. An increase of 18-oxocortisol and 18-hydroxycortisol was also observed in response to uPSEM-817 in two of the three clones, suggesting production of hybrid steroids in response to increased intracellular Na^+ concentration. This is consistent with results reported

for the overexpression of KCNJ5 harboring the p.Tyr158Ala mutation in HAC cells resulting in a significant increase of both 18-hydroxycortisol and 18-oxocortisol^{18,33}. However, despite similar depolarization of the cells in response to uPSEM-817 or AngII, our data suggest a delayed activation of mineralocorticoid biosynthesis in response to the modulation of intracellular Na⁺ concentration compared to AngII and K⁺ that could be due to the activation of specific signaling pathways. This hypothesis is supported by our finding of a specific gene expression signature associated with Na⁺ influx into the cells.

Interestingly, gene expression analysis revealed expression of *KCNJ5* in H295R-S2 α7-5HT3-R cells (Figure S12A), which remains unchanged after uPSEM-817 treatment. In this context, Na⁺ may act as an activator for the KCNJ5 channel³⁴ by binding to the C-terminal part of the channel, near a region also sensitive to the PtdIns(4,5)P₂, enhancing the sensitivity of the channels to PtdIns(4,5)P₂³⁵. The interaction of PtdIns(4,5)P₂ with the C-terminal part of GIRK4 has been shown to regulate its opening by stabilizing the structure of the pore³⁵. The resulting K⁺ extrusion may attenuate the activation of Ca²⁺ signaling and explain the delayed increased in aldosterone biosynthesis observed in response to uPSEM817.

If the role of *KCNJ5* mutations in inducing aldosterone biosynthesis has been clearly established, their role in promoting abnormal cell proliferation is still a matter of debate. In our model, we demonstrated that Na⁺ entry into the cells lead to decreased cell proliferation and increased apoptosis. This is in accordance with previous studies showing that expression of *KCNJ5* mutants in adrenocortical cells resulted in decreased cell proliferation associated in some cases with increased apoptosis^{18,20}. Choi *et al* postulated that the activation of Ca²⁺ signaling induced by *KCNJ5* mutations is responsible for both⁸ increased aldosterone biosynthesis and cell proliferation, and indeed some studies also reported an association between *KCNJ5* mutations and larger adenoma size^{29,30} and a positive correlation between

expression of Ki67, a marker of cell proliferation, and the diameter of APA harboring *KCNJ5* mutations²⁰. Specific factors overexpressed in APA harboring *KCNJ5* mutations^{36,37} have been suggested to possibly counteract the pro-apoptotic effect of these mutations²⁰ suggesting, the existence of compensatory mechanisms maintaining cell proliferation over long term. In particular, expression of Teratocarcinoma-Derived Growth Factor-1 (*TDGF-I*) and Vinsinin-like 1 (*VSNL1*), two genes with anti-apoptotic properties, were found to be upregulated in *KCNJ5* mutated APA^{38,39}. However, in our cell model the expression of *VSNL1* was not modified (Figure S12B) and *TDGF1* was not expressed at all. The increased expression of these genes may be a later event secondary to the development of an APA to compensate for Na⁺-induced cell death. Moreover, signaling pathway analyses revealed downregulation of genes involved in the G2/M checkpoint pathway and in the progression through the cell division cycle, probably contributing to the decrease of cell proliferation observed in our model. Alternatively, our data suggest that other mechanisms may be responsible for abnormal cell proliferation, leading to the development of APA. These include the presence of two hits, one responsible for cell proliferation and the other for autonomous aldosterone production. Recently, we and others identified risk alleles associated to PA in genome wide association studies. Within the identified genetic loci, some genes appear to modulate adrenal cortex homeostasis and may affect cell proliferation, eventually generating a propitious environment leading to the occurrence of somatic mutations^{40,41}. The two models are not mutually exclusive and may be linked together by mechanisms that remain to be identified. Finally, in FH-III it cannot be ruled out that Na⁺ entry induced by *KCNJ5* mutations may have an impact on cell proliferation during adrenal development, which could explain the bilateral hyperplasia observed in severe cases^{8,19}.

AngII and potassium both stimulate aldosterone biosynthesis by activating Ca²⁺ signaling, but through different mechanisms, resulting in only a partial overlap in the genes they induce. Similarly, uPSEM-817, by increasing intracellular Na⁺ levels, induces membrane

depolarization, which like potassium, leading to opening of voltage-gated Ca^{2+} channels and increase of intracellular Ca^{2+} concentration. However, uPSEM-817 also has unique effects, which account for the partial overlap in the differentially expressed genes induced by these three compounds. Gene expression profiles allowed us to identify a sodium-induced gene signature composed of 10 genes after 8h of treatment with uPSEM-817 (Figure S9) and 14 genes after 24h of treatment (Figure S10). Interestingly, among these lists of genes, some are involved in cell cycle regulation, proliferation and apoptosis. Hence, the expression of *RBMS2* and *PTPRU*, two genes involved in the control of cell cycle progression⁴² and cell proliferation^{43,44} respectively, was decreased after 8h or 24h while the expression of *CDK10*, a Cdc2-related kinase involved in the regulation of the G2/M phase of the cell cycle, was increased. However, the role of CDK10 in regulating cell proliferation is not clear, as some studies suggest a role of CDK10 in cell proliferation activation⁴⁵⁻⁴⁷, while others report a tumor suppressor role for CDK10 through inhibition of cell proliferation^{48,49}. The identification of these genes in the Na^+ -signature supports our results showing an inhibitory effect of uPSEM-817 on cell proliferation. Among the genes belonging to the Na^+ signature after 8h of treatment with uPSEM-817, *HPX* expression was found to be upregulated. *HPX* encodes hemopexin, a protein with high binding affinity for heme. Interestingly, CYP11B2 and other cytochromes P450 enzymes use heme as cofactor required for their activity. The availability of heme has been shown to affect aldosterone and corticosterone biosynthesis in rats⁵⁰. Our transcriptomic data revealed a significant increase of *HPX* expression in APA harboring a *KCNJ5* mutation²⁹ and a recent study reported also increased expression of *HPX* associated with CpG hypomethylation⁵¹ in APA compared to adjacent adrenal gland suggesting a role of *HPX* in APA development potentially through the regulation of aldosterone biosynthesis. Similarly, the expression of *MC2R*, the melanocortin 2 receptor, was found to be increased in APA associated with CpG hypomethylation⁵¹. Gene expression profiling of H295R-S2 α 7-5HT3-R cells treated

with either AngII, K⁺ or uPSEM-817 revealed also a significant increase of *MC2R* expression; and a previous study reported higher expression of *MC2R* in APA compared to control adrenals⁵². Finally, a recent work of our laboratory shows that expression of MC2R in APA was more frequently found in regions expressing CYP11B2⁵³, suggesting a potential role in regulating aldosterone biosynthesis. Moreover, the existence of a continuum of PA and dysregulated aldosterone production, prominently influenced by ACTH, has recently been described⁵⁴.

In conclusion, we demonstrate that H295R-S2 α7-5HT3-R cells are a new cell model in which intracellular Ca²⁺ concentration can be modulated on “demand”, reproducing the major features of cells harbouring *KCNJ5* mutations. The stimulation of Na⁺ entry into the cells leads to cell membrane depolarization, Ca²⁺ entry into the cells, activation of Ca²⁺ signaling, increased expression of *CYP11B2* and stimulation of the mineralocorticoid biosynthesis pathway. This is associated with a decrease of cell proliferation and an increase of apoptosis, indicating that additional events may be required for the development of APA. RNA sequencing revealed that Na⁺ entry into the cells is responsible for a specific transcriptomic signature that may explain some of the features of APA carrying a *KCNJ5* mutations. This cellular model thus provides important new insight into the mechanisms leading to PA development, uncovering new mechanisms involved in the disease, thereby paving the way for new therapeutic approaches in primary aldosteronism.

The strengths of our study are multiple. First, the model provides a novel and highly valuable tool for studying the early events that occur following a mutational event leading to Na⁺ entry into the cells, such as mutations affecting *KCNJ5*⁸ but also mutations affecting *SLC30A1*¹⁵, *ATPIAI*^{9,16} and *MCOLN3*⁵⁵. Second, the cell model allows following dynamic changes in cell proliferation and function and to explore molecular mechanisms and specific

transcriptional changes induced by mutations in PA. Importantly, these events cannot be studied in human tissues from patients with APA, as they only provide a snapshot at a given moment of the development of the disease. Indeed, we were able to show that while modification of steroid biosynthesis occurs very rapidly, alterations in the cellular sodium balance result in reduced cell proliferation and increased apoptosis, in accordance with data from the literature¹⁸. However, we cannot exclude the possibility that, at a later stage of development of APA, the constitutive activation of Ca^{2+} signaling might stimulate cell proliferation. Another significant finding of our study was the identification of specific pathways and signatures associated with the modification of Na^+ influx. While some pathways, such as Aldosterone biosynthesis and secretion, calcium signaling and cell proliferation, were further explored, others remain to be investigated and will be the scope of future research. Moreover, this innovative cellular model offers a valuable tool for evaluating the molecular effects of novel therapeutic strategies for PA, particularly the application of novel aldosterone synthase inhibitors.

Limitations of our study are related to possible biases in interpreting proliferation studies in our model. Indeed, these cells are generated from H295R-S2 cells, which derive from an adrenocortical adenoma carrying TP53 and β -catenin mutations. Since β -catenin signaling is known to promote cell proliferation in various tumors, this model may be suboptimal for investigating positive effects on proliferation. Nevertheless, we have demonstrated that the activation of Ca^{2+} signaling, through modulation of Na^+ entry into the cells is achievable within this context. Therefore, the presence of β -catenin mutations does not pose an obstacle to these specific investigations. An additional limitation may be the lack of the microenvironment of steroidogenic cells; further studies in integrated mouse models will be necessary to establish the natural history of PA development.

Perspectives

Using a chemogenetic approach allowing the modulation of sodium influx “on demand”, we have generated a new cell model which replicates the main characteristics of *KCNJ5*-mutated APAs and provides new insights into the mechanisms responsible for their development. Our results show that modulation of intracellular ionic balance leads to cell membrane depolarization, activation of Ca^{2+} signaling and enhanced steroid biosynthesis, associated with a decrease in cell viability and an increase in apoptosis, indicating that additional events may be required for the development of an APA with *KCNJ5* mutation.

This innovative model could be used to test the molecular impact of new treatments for PA *in vitro*. Additionally, applying this chemogenetic approach could also enable the development of a new inducible mouse model of PA, providing a valuable tool for dissecting the mechanisms underlying APA development and for evaluating new therapeutic strategies.

Acknowledgments

Acknowledgments

None

Sources of Funding

This work was funded through institutional support from INSERM, by the Agence Nationale pour la Recherche (ANR-18-CE93-0003-01), the Fondation pour la Recherche Médicale (EQU201903007864), the European Union's Horizon 2020 research and innovation programme under the Marie Skłodowska-Curie grant agreement No. 954798 (MINDSHIFT ITN), for which M-C.Zennaro. is principal investigator, and by a grant from the Leducq Foundation (18CVD05) for J-S.Hulot. Research in D. Penton's laboratory was financed by the Swiss National Foundation for Science (CRSII-222773) and by the University Research Priority Program of the University of Zurich (URPP) ITINERARE-Innovative Therapies in Rare Diseases.

Disclosures

None

References

1. Spat A, Hunyady L. Control of aldosterone secretion: a model for convergence in cellular signaling pathways. *Physiol Rev.* 2004;84:489–539.
2. Fernandes-Rosa FL, Boulkroun S, Zennaro M-C. Genetic and Genomic Mechanisms of Primary Aldosteronism. *Trends in Molecular Medicine* [Internet]. 2020 [cited 2020 Jul 7]; Available from: <http://www.sciencedirect.com/science/article/pii/S1471491420301349>
3. Hannemann A, Bidlingmaier M, Friedrich N, Manolopoulou J, Spyroglou A, Volzke H, Beuschlein F, Seissler J, Rettig R, Felix SB, et al. Screening for primary aldosteronism in hypertensive subjects: results from two German epidemiological studies. *European Journal of Endocrinology.* 2012;167:7–15.
4. Monticone S, Burrello J, Tizzani D, Bertello C, Viola A, Buffolo F, Gabetti L, Mengozzi G, Williams TA, Rabbia F, et al. Prevalence and Clinical Manifestations of Primary Aldosteronism Encountered in Primary Care Practice. *Journal of the American College of Cardiology.* 2017;69:1811–1820.
5. Käyser SC, Dekkers T, Groenewoud HJ, van der Wilt GJ, Carel Bakx J, van der Wel MC, Hermus AR, Lenders JW, Deinum J. Study Heterogeneity and Estimation of Prevalence of Primary Aldosteronism: A Systematic Review and Meta-Regression Analysis. *J Clin Endocrinol Metab.* 2016;101:2826–2835.
6. Xu Z, Yang J, Hu J, Song Y, He W, Luo T, Cheng Q, Ma L, Luo R, Fuller PJ, et al. Primary Aldosteronism in Patients in China With Recently Detected Hypertension. *J Am Coll Cardiol.* 2020;75:1913–1922.
7. Savard S, Amar L, Plouin PF, Steichen O. Cardiovascular complications associated with primary aldosteronism: a controlled cross-sectional study. *Hypertension.* 2013;62:331–6.

8. Choi M, Scholl UI, Yue P, Bjorklund P, Zhao B, Nelson-Williams C, Ji W, Cho Y, Patel A, Men CJ, et al. K⁺ channel mutations in adrenal aldosterone-producing adenomas and hereditary hypertension. *Science*. 2011;331:768–72.
9. Azizan EA, Poulsen H, Tuluc P, Zhou J, Clausen MV, Lieb A, Maniero C, Garg S, Bochukova EG, Zhao W, et al. Somatic mutations in ATP1A1 and CACNA1D underlie a common subtype of adrenal hypertension. *Nature genetics*. 2013;45:1055–60.
10. Scholl UI, Goh G, Stolting G, de Oliveira RC, Choi M, Overton JD, Fonseca AL, Korah R, Starker LF, Kunstman JW, et al. Somatic and germline CACNA1D calcium channel mutations in aldosterone-producing adenomas and primary aldosteronism. *Nature genetics*. 2013;45:1050–4.
11. Scholl UI, Stolting G, Nelson-Williams C, Vichot AA, Choi M, Loring E, Prasad ML, Goh G, Carling T, Juhlin CC, et al. Recurrent gain of function mutation in calcium channel CACNA1H causes early-onset hypertension with primary aldosteronism. *Elife*. 2015;4:e06315.
12. Daniil G, Fernandes-Rosa FL, Chemin J, Blesneac I, Beltrand J, Polak M, Jeunemaitre X, Boulkroun S, Amar L, Strom TM, et al. CACNA1H Mutations Are Associated With Different Forms of Primary Aldosteronism. *EBioMedicine*. 2016;13:225–236.
13. Fernandes-Rosa FL, Daniil G, Orozco IJ, Göppner C, El Zein R, Jain V, Boulkroun S, Jeunemaitre X, Amar L, Lefebvre H, et al. A gain-of-function mutation in the CLCN2 chloride channel gene causes primary aldosteronism. *Nat Genet*. 2018;50:355–361.
14. Scholl UI, Stolting G, Schewe J, Thiel A, Tan H, Nelson-Williams C, Vichot AA, Jin SC, Loring E, Untiet V, et al. CLCN2 chloride channel mutations in familial hyperaldosteronism type II. *Nat Genet*. 2018;50:349–354.

15. Rege J, Bandulik S, Nanba K, Kosmann C, Blinder AR, Plain A, Vats P, Kumar-Sinha C, Lerario AM, Else T, et al. Somatic SLC30A1 mutations altering zinc transporter ZnT1 cause aldosterone-producing adenomas and primary aldosteronism. *Nat Genet*. 2023;55:1623–1631.
16. Beuschlein F, Boulkroun S, Osswald A, Wieland T, Nielsen HN, Lichtenauer UD, Penton D, Schack VR, Amar L, Fischer E, et al. Somatic mutations in ATP1A1 and ATP2B3 lead to aldosterone-producing adenomas and secondary hypertension. *Nat Genet*. 2013;45:440–444.
17. Scholl UI, Nelson-Williams C, Yue P, Grekin R, Wyatt RJ, Dillon MJ, Couch R, Hammer LK, Harley FL, Farhi A, et al. Hypertension with or without adrenal hyperplasia due to different inherited mutations in the potassium channel KCNJ5. *Proc Natl Acad Sci U S A*. 2012;109:2533–8.
18. Oki K, Plonczynski MW, Luis Lam M, Gomez-Sanchez EP, Gomez-Sanchez CE. Potassium channel mutant KCNJ5 T158A expression in HAC-15 cells increases aldosterone synthesis. *Endocrinology*. 2012;153:1774–82.
19. Mulatero P, Tauber P, Zennaro MC, Monticone S, Lang K, Beuschlein F, Fischer E, Tizzani D, Pallauf A, Viola A, et al. KCNJ5 mutations in European families with nonglucocorticoid remediable familial hyperaldosteronism. *Hypertension*. 2012;59:235–40.
20. Yang Y, Gomez-Sanchez CE, Jaquin D, Aristizabal Prada ET, Meyer LS, Knosel T, Schneider H, Beuschlein F, Reincke M, Williams TA. Primary Aldosteronism: KCNJ5 Mutations and Adrenocortical Cell Growth. *Hypertension*. 2019;74:809–816.
21. Magnus CJ, Lee PH, Atasoy D, Su HH, Looger LL, Sternson SM. Chemical and genetic engineering of selective ion channel-ligand interactions. *Science*. 2011;333:1292–6.

22. Magnus CJ, Lee PH, Bonaventura J, Zemla R, Gomez JL, Ramirez MH, Hu X, Galvan A, Basu J, Michaelides M, et al. Ultrapotent chemogenetics for research and potential clinical applications. *Science*. 2019;364.
23. Wang T, Rowland JG, Parmar J, Nesterova M, Seki T, Rainey WE. Comparison of aldosterone production among human adrenocortical cell lines. *Horm Metab Res*. 2012;44:245–50.
24. Bustin SA, Benes V, Garson JA, Hellemans J, Huggett J, Kubista M, Mueller R, Nolan T, Pfaffl MW, Shipley GL, et al. The MIQE guidelines: minimum information for publication of quantitative real-time PCR experiments. *Clin Chem*. 2009;55:611–22.
25. Yang T, He M, Zhang H, Barrett PQ, Hu C. L- and T-type calcium channels control aldosterone production from human adrenals. *J Endocrinol*. 2020;244:237–247.
26. Barrett PQ, Guagliardo NA, Klein PM, Hu C, Breault DT, Beenhakker MP. Role of voltage-gated calcium channels in the regulation of aldosterone production from zona glomerulosa cells of the adrenal cortex. *J Physiol*. 2016;594:5851–5860.
27. Sherman BT, Hao M, Qiu J, Jiao X, Baseler MW, Lane HC, Imamichi T, Chang W. DAVID: a web server for functional enrichment analysis and functional annotation of gene lists (2021 update). *Nucleic Acids Research*. 2022;50:W216–W221.
28. Huang DW, Sherman BT, Lempicki RA. Systematic and integrative analysis of large gene lists using DAVID bioinformatics resources. *Nat Protoc*. 2009;4:44–57.
29. Boulkroun S, Beuschlein F, Rossi GP, Golib-Dzib JF, Fischer E, Amar L, Mulatero P, Samson-Couterie B, Hahner S, Quinkler M, et al. Prevalence, Clinical, and Molecular Correlates of KCNJ5 Mutations in Primary Aldosteronism. *Hypertension*. 2012;59:592–8.
30. Fernandes-Rosa FL, Williams TA, Riester A, Steichen O, Beuschlein F, Boulkroun S,

Strom TM, Monticone S, Amar L, Meatchi T, et al. Genetic Spectrum and Clinical Correlates of Somatic Mutations in Aldosterone-Producing Adenoma. *Hypertension*. 2014;64:354–361.

31. Lenzini L, Rossitto G, Maiolino G, Letizia C, Funder JW, Rossi GP. A Meta-Analysis of Somatic KCNJ5 K(+) Channel Mutations In 1636 Patients With an Aldosterone-Producing Adenoma. *J Clin Endocrinol Metab*. 2015;100:E1089-95.

32. Mangelis A, Dieterich P, Peitzsch M, Richter S, Jühlen R, Hübner A, Willenberg HS, Deussen A, Lenders JWM, Eisenhofer G. Computational analysis of liquid chromatography-tandem mass spectrometric steroid profiling in NCI H295R cells following angiotensin II, forskolin and abiraterone treatment. *J Steroid Biochem Mol Biol*. 2016;155:67–75.

33. Hattangady NG, Karashima S, Yuan L, Ponce-Balbuena D, Jalife J, Gomez-Sanchez CE, Auchus RJ, Rainey WE, Else T. Mutated KCNJ5 activates the acute and chronic regulatory steps in aldosterone production. *J Mol Endocrinol*. 2016;57:1–11.

34. Sui JL, Chan KW, Logothetis DE. Na⁺ activation of the muscarinic K⁺ channel by a G-protein-independent mechanism. *J Gen Physiol*. 1996;108:381–391.

35. Rosenhouse-Dantsker A, Sui JL, Zhao Q, Rusinova R, Rodríguez-Menchaca AA, Zhang Z, Logothetis DE. A sodium-mediated structural switch that controls the sensitivity of Kir channels to PtdIns(4,5)P(2). *Nat Chem Biol*. 2008;4:624–631.

36. Azizan EA, Lam BY, Newhouse SJ, Zhou J, Kuc RE, Clarke J, Happerfield L, Marker A, Hoffman GJ, Brown MJ. Microarray, qPCR, and KCNJ5 sequencing of aldosterone-producing adenomas reveal differences in genotype and phenotype between zona glomerulosa- and zona fasciculata-like tumors. *J Clin Endocrinol Metab*. 2012;97:E819-29.

37. Akerstrom T, Willenberg HS, Cupisti K, Ip J, Backman S, Moser A, Maharjan R, Robinson B, Iwen KA, Dralle H, et al. Novel somatic mutations and distinct molecular

signature in aldosterone-producing adenomas. *Endocr Relat Cancer*. 2015;22:735–44.

38. Williams TA, Monticone S, Morello F, Liew CC, Mengozzi G, Pilon C, Asioli S, Sapino A, Veglio F, Mulatero P. Teratocarcinoma-derived growth factor-1 is upregulated in aldosterone-producing adenomas and increases aldosterone secretion and inhibits apoptosis in vitro. *Hypertension*. 2010;55:1468–75.
39. Williams TA, Monticone S, Crudo V, Warth R, Veglio F, Mulatero P. Visinin-Like 1 Is Upregulated in Aldosterone-Producing Adenomas With KCNJ5 Mutations and Protects From Calcium-Induced Apoptosis. *Hypertension*. 2012;59:833–839.
40. Le Floch E, Cosentino T, Larsen CK, Beuschlein F, Reincke M, Amar L, Rossi G-P, De Sousa K, Baron S, Chantalat S, et al. Identification of risk loci for primary aldosteronism in genome-wide association studies. *Nat Commun*. 2022;13:5198.
41. Naito T, Inoue K, Sonehara K, Baba R, Kodama T, Otagaki Y, Okada A, Itcho K, Kobuke K, Kishimoto S, et al. Genetic Risk of Primary Aldosteronism and Its Contribution to Hypertension: A Cross-Ancestry Meta-Analysis of Genome-Wide Association Studies. *Circulation*. 2023;147:1097–1109.
42. Sun X, Hu Y, Wu J, Shi L, Zhu L, Xi P-W, Wei J-F, Ding Q. RBMS2 inhibits the proliferation by stabilizing P21 mRNA in breast cancer. *J Exp Clin Cancer Res*. 2018;37:298.
43. Zhu Z, Liu Y, Li K, Liu J, Wang H, Sun B, Xiong Z, Jiang H, Zheng J, Hu Z. Protein tyrosine phosphatase receptor U (PTPRU) is required for glioma growth and motility. *Carcinogenesis*. 2014;35:1901–1910.
44. Liu Y, Zhu Z, Xiong Z, Zheng J, Hu Z, Qiu J. Knockdown of protein tyrosine phosphatase receptor U inhibits growth and motility of gastric cancer cells. *Int J Clin Exp Pathol*. 2014;7:5750–5761.

45. Li S, MacLachlan TK, De Luca A, Claudio PP, Condorelli G, Giordano A. The cdc-2-related kinase, PISSLRE, is essential for cell growth and acts in G2 phase of the cell cycle. *Cancer Res.* 1995;55:3992–3995.
46. Poon SSS, Wong JT, Saunders DN, Ma QC, McKinney S, Fee J, Aparicio SAJR. Intensity calibration and automated cell cycle gating for high-throughput image-based siRNA screens of mammalian cells. *Cytometry A.* 2008;73:904–917.
47. Guen VJ, Gamble C, Perez DE, Bourassa S, Zappel H, Gärtner J, Lees JA, Colas P. STAR syndrome-associated CDK10/Cyclin M regulates actin network architecture and ciliogenesis. *Cell Cycle.* 2016;15:678–688.
48. Yu J-H, Zhong X-Y, Zhang W-G, Wang Z-D, Dong Q, Tai S, Li H, Cui Y-F. CDK10 functions as a tumor suppressor gene and regulates survivability of biliary tract cancer cells. *Oncol Rep.* 2012;27:1266–1276.
49. Zhong X, Xu X, Yu J, Jiang G, Yu Y, Tai S, Wang Z, Cui Y. Clinical and biological significance of Cdk10 in hepatocellular carcinoma. *Gene.* 2012;498:68–74.
50. Martini CN, Vaena de Avalos SG, Romero DG, San Martin de Viale L, Vila Mde C. Heme availability affects corticosterone and aldosterone biosynthesis in rat adrenal. *Steroids.* 1997;62:767–70.
51. Murakami M, Yoshimoto T, Nakabayashi K, Tsuchiya K, Minami I, Bouchi R, Izumiya H, Fujii Y, Abe K, Tayama C, et al. Integration of transcriptome and methylome analysis of aldosterone-producing adenomas. *Eur J Endocrinol.* 2015;173:185–195.
52. Ye P, Mariniello B, Mantero F, Shibata H, Rainey WE. G-protein-coupled receptors in aldosterone-producing adenomas: a potential cause of hyperaldosteronism. *J Endocrinol.* 2007;195:39–48.

53. De Sousa K, Abdellatif AB, Giscos-Douriez I, Meatchi T, Amar L, Fernandes-Rosa FL, Boulkroun S, Zennaro M-C. Colocalization of Wnt/β-Catenin and ACTH Signaling Pathways and Paracrine Regulation in Aldosterone-producing Adenoma. *J Clin Endocrinol Metab.* 2022;107:419–434.
54. Parksook WW, Brown JM, Omata K, Tezuka Y, Ono Y, Satoh F, Tsai LC, Niebuhr Y, Milks J, Moore A, et al. The Spectrum of Dysregulated Aldosterone Production: An International Human Physiology Study. *J Clin Endocrinol Metab.* 2024;dgae145.
55. van Rooyen D, Bandulik S, Coon G, Laukemper M, Kumar-Sinha C, Udager AM, Lee C, Wachtel H, Cohen DL, Luther JM, et al. Somatic Mutations in MCOLN3 in Aldosterone-Producing Adenomas cause Primary Aldosteronism. *bioRxiv.* 2024;2024.10.20.619295.

Novelty and relevance

What is new?

Herein, we have developed a novel cell model in which intracellular Ca^{2+} concentration can be modulated on demand, through modulation of sodium entry, reproducing the major characteristics of cells harboring a *KCNJ5* mutations.

We demonstrate that Na^+ entry into the cells results, on one hand, in cell membrane depolarization, Ca^{2+} influx, activation of Ca^{2+} signaling leading to increased expression of *CYP11B2* and stimulation of mineralocorticoid biosynthesis and, on the other hand, to a decrease in cell proliferation and an increase in apoptosis,

We show that Na^+ influx leads to a specific transcriptome signature that may explain some of the peculiar features of aldosterone producing adenoma carrying *KCNJ5* mutations compared to other genetic abnormalities.

What is relevant?

While the role of *KCNJ5* mutations in promoting autonomous aldosterone biosynthesis has been clearly established, their role in promoting also abnormal cell proliferation remains to be established. Our study demonstrates that, *KCNJ5* mutations are not able to promote both autonomous aldosterone production and cell proliferation, suggesting that additional events may be required for adenoma development.

Clinical/pathophysiological implications?

This cellular model offers valuable new insights into the mechanisms leading to primary aldosteronism development, revealing novel processes involved in the disease and paving the way for new therapeutic approaches in PA.

Supplemental material

Expanded Materials and Methods

Tables S1-S15

Figures S1-S13

Table 1. Steroid profiles in H295R S2 cells expressing the α 7-5HT3-R in response to AngII (10^{-8} M), K⁺ (12mM) and uPSEM-817 (10^{-9} to 10^{-5} M).

Characteristics	Time	AngII (10^{-8} M)	K ⁺ (12mM)	PSEM (10^{-9} M)	PSEM (10^{-8} M)	PSEM (10^{-7} M)	PSEM (10^{-6} M)	PSEM (10^{-5} M)
Pregnenolone	8h	2.622 \pm 0.176 ****	2.458 \pm 0.203 ****	1.071 \pm 0.025	1.035 \pm 0.024	1.269 \pm 0.031 ****	1.254 \pm 0.037 ***	1.489 \pm 0.066 ****
	24h	0.441 \pm 0.023 ****	0.813 \pm 0.038	1.031 \pm 0.036	1.045 \pm 0.041	1.485 \pm 0.206	1.419 \pm 0.157 *	1.643 \pm 0.065 ***
Progesterone	8h	4.005 \pm 0.366 ****	3.112 \pm 0.296 **	1.167 \pm 0.020	1.150 \pm 0.016	1.422 \pm 0.065 ***	1.453 \pm 0.065 ****	1.652 \pm 0.077 ****
	24h	0.330 \pm 0.022 ****	0.533 \pm 0.036 ****	1.058 \pm 0.058	1.002 \pm 0.056	1.165 \pm 0.045	1.115 \pm 0.052	1.196 \pm 0.048 *
11-deoxycorticosterone	8h	4.100 \pm 0.478 ***	3.811 \pm 0.350 **	1.025 \pm 0.046	0.981 \pm 0.060	1.272 \pm 0.049 *	1.241 \pm 0.039 *	1.378 \pm 0.060 **
	24h	0.409 \pm 0.044 ****	0.828 \pm 0.051	1.055 \pm 0.040	1.012 \pm 0.024	1.219 \pm 0.041 **	1.197 \pm 0.056 **	1.349 \pm 0.048 ****
18-hydroxy 11-deoxycorticosterone	8h	2.761 \pm 0.205 ***	2.585 \pm 0.238 **	1.122 \pm 0.019	1.114 \pm 0.023	1.260 \pm 0.055 ***	1.353 \pm 0.064 ****	1.455 \pm 0.038 ****
	24h	2.467 \pm 0.193 ****	2.235 \pm 0.198 ****	0.982 \pm 0.038	0.973 \pm 0.034	1.234 \pm 0.041 *	1.271 \pm 0.081	1.404 \pm 0.101 **
Corticosterone	8h	2.515 \pm 0.179 ****	2.424 \pm 0.245 ****	1.108 \pm 0.035	1.148 \pm 0.036	1.294 \pm 0.074	1.090 \pm 0.187	1.021 \pm 0.188
	24h	2.329 \pm 0.268 ****	1.983 \pm 0.183 **	0.984 \pm 0.051	1.002 \pm 0.055	1.169 \pm 0.033 *	1.174 \pm 0.032 **	1.302 \pm 0.026 ****
18-hydroxycortisol	8h	0.794 \pm 0.090	0.921 \pm 0.112	0.944 \pm 0.057	0.754 \pm 0.126	0.910 \pm 0.053	0.894 \pm 0.037	1.314 \pm 0.249
	24h	2.200 \pm 0.575	8.049 \pm 2.958 **	2.203 \pm 0.557	2.241 \pm 0.595	3.047 \pm 1.206	2.126 \pm 0.691	2.086 \pm 0.622
18-oxocortisol	8h	1.046 \pm 0.094	1.131 \pm 0.126	0.937 \pm 0.043	0.798 \pm 0.075	0.929 \pm 0.028	1.068 \pm 0.102	1.633 \pm 0.355
	24h	2.200 \pm 0.575	8.049 \pm 2.958 **	2.203 \pm 0.557	2.241 \pm 0.595	3.047 \pm 1.206	2.126 \pm 0.691	2.086 \pm 0.622
18-hydroxycorticosterone	8h	1.927 \pm 0.172 ***	2.088 \pm 0.156 ****	1.125 \pm 0.033	1.125 \pm 0.052	1.231 \pm 0.051 *	1.003 \pm 0.108	0.835 \pm 0.063
	24h	3.496 \pm 0.400 ****	2.456 \pm 0.341 **	0.989 \pm 0.074	1.004 \pm 0.094	1.177 \pm 0.157	0.891 \pm 0.102	0.818 \pm 0.085
Aldosterone	8h	2.454 \pm 0.238 **	2.580 \pm 0.273 ***	0.914 \pm 0.040	0.927 \pm 0.038	1.024 \pm 0.054	1.187 \pm 0.063	1.388 \pm 0.062
	24h	12.13 \pm 4.007 ****	6.046 \pm 1.657 **	0.946 \pm 0.043	1.035 \pm 0.082	1.495 \pm 0.211	1.459 \pm 0.138 **	1.436 \pm 0.135 **
17-hydroxyprogesterone	8h	2.761 \pm 0.351 ****	2.535 \pm 0.242 ***	1.187 \pm 0.027 *	1.141 \pm 0.035	1.334 \pm 0.059 ****	1.325 \pm 0.051 ****	1.589 \pm 0.041 ****
	24h	0.243 \pm 0.009 ****	0.896 \pm 0.034 **	1.052 \pm 0.038	0.975 \pm 0.041	1.068 \pm 0.034	1.049 \pm 0.032	1.230 \pm 0.030 **
11-deoxycortisol	8h	1.586 \pm 0.147 ***	1.706 \pm 0.105 ***	1.026 \pm 0.033	0.995 \pm 0.056	1.087 \pm 0.038	1.064 \pm 0.035	1.079 \pm 0.039
	24h	1.065 \pm 0.046	0.626 \pm 0.064 ****	1.016 \pm 0.025	0.985 \pm 0.030	1.096 \pm 0.041	1.073 \pm 0.052	1.060 \pm 0.046
Cortisol	8h	1.093 \pm 0.061	1.066 \pm 0.056	1.119 \pm 0.082	1.157 \pm 0.058	1.126 \pm 0.081	1.051 \pm 0.057	1.003 \pm 0.055
	24h	2.541 \pm 0.310 ****	1.923 \pm 0.251 **	0.974 \pm 0.033	1.034 \pm 0.041	1.161 \pm 0.080	1.194 \pm 0.095	1.199 \pm 0.076
21-deoxycortisol	8h	1.546 \pm 0.135 *	1.443 \pm 0.139	1.046 \pm 0.074	1.059 \pm 0.146	0.968 \pm 0.143	0.926 \pm 0.163	1.863 \pm 0.548
	24h	0.852 \pm 0.121	1.954 \pm 0.115 ****	1.151 \pm 0.120	1.107 \pm 0.098	1.345 \pm 0.162	1.195 \pm 0.073	0.941 \pm 0.122
Delta-4-androstenedione	8h	1.450 \pm 0.123 *	1.541 \pm 0.131 **	1.001 \pm 0.033	0.978 \pm 0.085	1.113 \pm 0.039	1.069 \pm 0.034	1.246 \pm 0.038 **
	24h	0.482 \pm 0.046 ****	1.146 \pm 0.055	1.049 \pm 0.032	1.003 \pm 0.027	1.098 \pm 0.047	0.985 \pm 0.039	1.104 \pm 0.041

Results are expressed as fold induction over untreated cells expressing the α 7-5HT3-R (set as 1, not shown) and represent mean \pm SEM of the three clones, compared with ANOVA followed by Bonferroni when data presented for Gaussian distribution and Kruskal–Wallis followed by Dunn's test for non-Gaussian distribution. Cells treated with AngII and K⁺ and cells treated with uPSEM-817 (PSEM) were analyzed separately. n=9/condition except for 18-oxocortisol (n=6) and 18-hydroxycortisol (n=6).

****, p ≤ 0.0001; ***, p ≤ 0.001; **, p ≤ 0.01, *, p ≤ 0.05

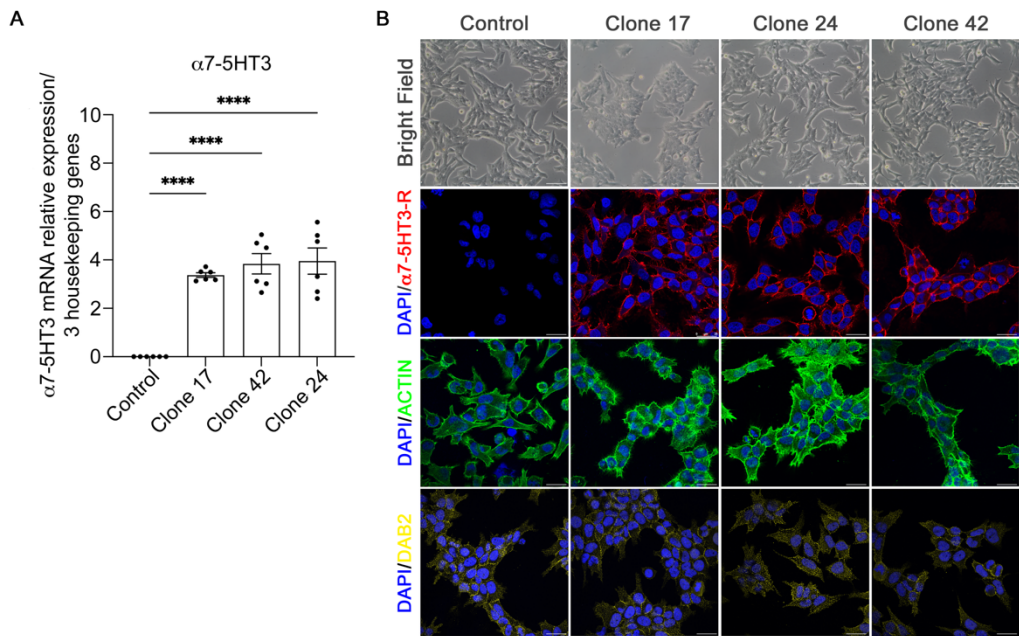


Figure 1. Morphological characterization of α7-5HT3-R expressing cells. The expression of α7-5HT3-R was investigated in control cells, expressing an empty vector, and in three selected clones, 17, 24 and 42. **(A)** mRNA expression of α7-5HT3-R was investigated by RT-qPCR, n=6 for each clone **(B)** Morphological characteristics of control and α7-5HT3-R expressing cells were evaluated by immunofluorescence. Bright field images revealed no structural difference between cells. DAPI nuclear staining is shown in blue, α-bungarotoxin (α7-5HT3-R) in red, Phalloidin (actin) in green and dab2 in yellow. P values were determined by one-way ANOVA followed by Bonferroni post-hoc comparisons tests, ***, p<0,0001, Bar represents 20μm

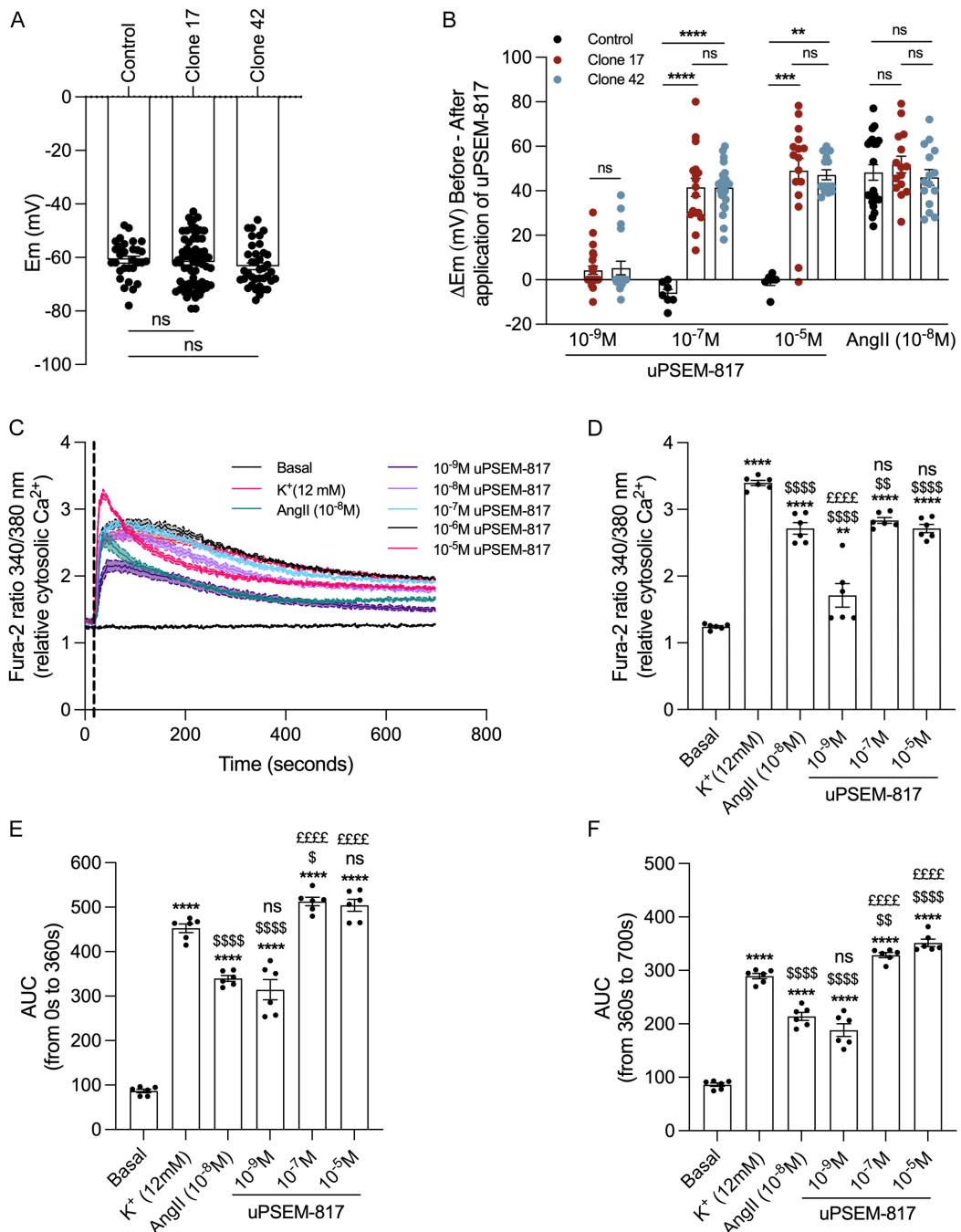


Figure 2. Functional characterization of α7-5HT3-R expressing cells. (A and B) Perforated patch clamp experiments were performed on clones 17 and 42 to determine the membrane potential of cells in basal condition, n=15-21 (A) or after stimulation with different concentrations of uPSEM-817 (10^{-9} , 10^{-7} and 10^{-5} M) and AngII (10^{-8} M), n=7-23 (B). (C) Ca²⁺ entry into the cells was evaluated using Fura-2 AM assay for 700s. Representative traces of intracellular Ca²⁺ responses to 10^{-8} M AngII, 12mM K⁺ and 10^{-9} to 10^{-5} M uPSEM-817 (Clone 17), n=6 (D) Determination of the maximum Fura-2 ratio 340/380nm in response to 10^{-8} M AngII, 12mM K⁺ and 10^{-9} , 10^{-7} and 10^{-5} M uPSEM-817 (Clone 17), n=6. (E) Area under the curve (AUC) was determined to assess whether treatment with PSEM induced Ca²⁺ entry into the cells. The AUC was determined between 0 and 360s to determine the intracellular Ca²⁺ variation during the peak response (left panel) and between 360s and 700s to determine the steady-state response (right panel) (Clone 17). n=6, P values were determined by t-test or one-

way ANOVA followed by Bonferroni post-hoc comparisons tests, * basal vs K⁺, AngII or PSEM, \$ K⁺ vs AngII or PSEM, £ AngII vs PSEM \$; p<0,05; \$\$, p<0,01, ns AngII vs 10⁻⁹M PSEM (left and right panel), K⁺ vs 10⁻⁵M PSEM (right panel); ****, p<0,0001; ns: not significant. The dotted line indicates the time of injection of uPSEM-817, AngII or K⁺.

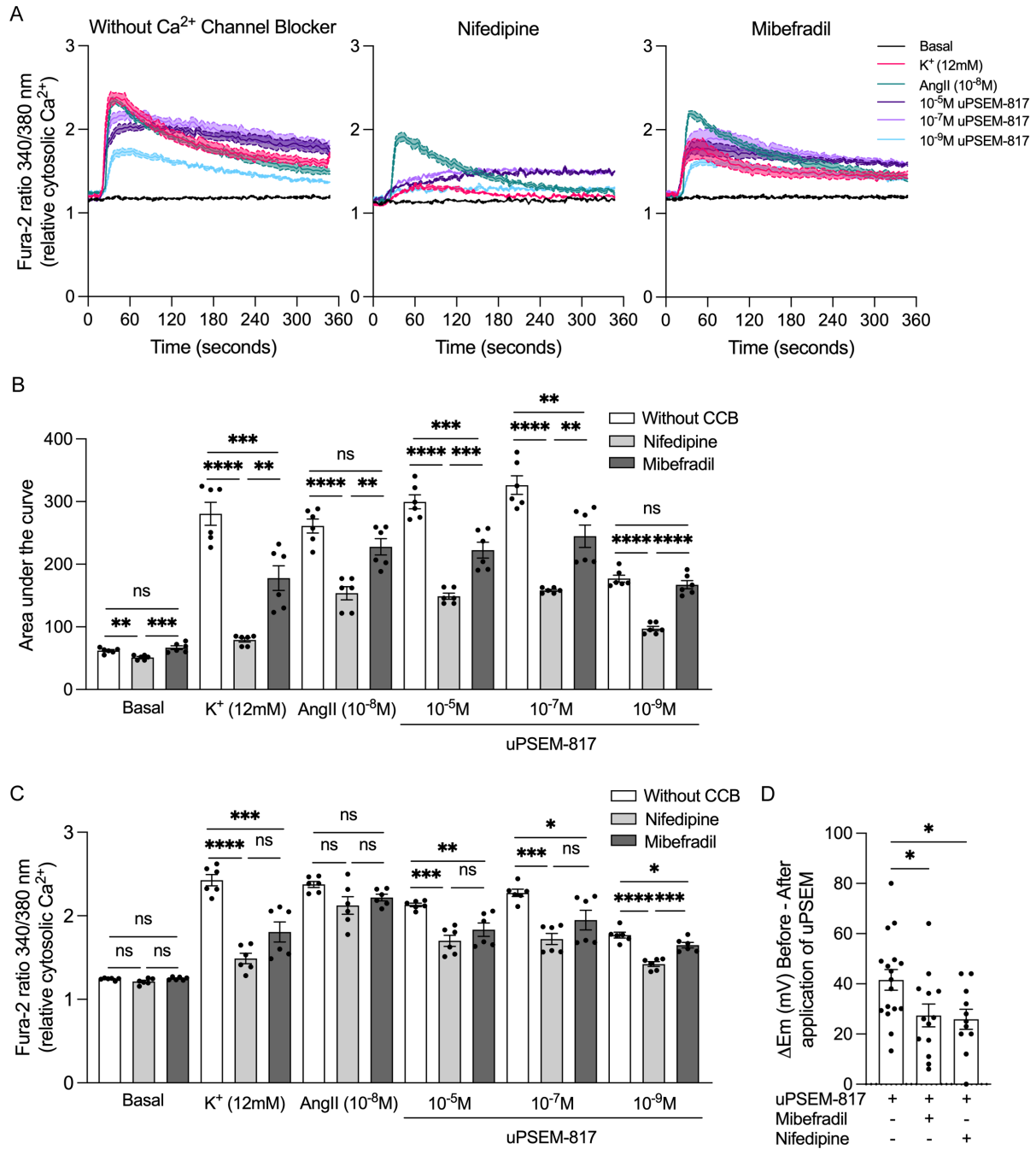


Figure 3. Inhibition of Ca^{2+} entry using Nifedipine or Mibepradil. (A) Representative traces of intracellular Ca^{2+} responses to 10^{-8}M AngII, 12mM K^+ and 10^{-9} , 10^{-7} and 10^{-5}M uPSEM-817 after pre-treatment with Nifedipine (left), or Mibepradil (right) (Clone 17); n=6. (B) Determination of the maximum Fura-2 ratio 340/380nm in response to uPSEM-817, AngII and K^+ after pre-treatment with nifedipine (red) or mibepradil (blue) or without pre-treatment (black) (Clone 17); n=6. (C) Illustration of the $[\text{Ca}^{2+}]_i$ signaling, illustrated by the determination of the AUC assessed for 360s, in response to uPSEM-817, AngII and K^+ after pre-treatment with nifedipine (red) or mibepradil (blue) or without pre-treatment (black) (Clone 17); n=6. (D) Path clamp recordings of cells treated with uPSEM-817 and/or nifedipine or mibepradil (Clone 17). n=11-17, P values were determined by one-way ANOVA followed by Bonferroni post-hoc comparisons tests, *, p<0.05; **, p<0.01; ***, p<0.001; ****, p<0.0001

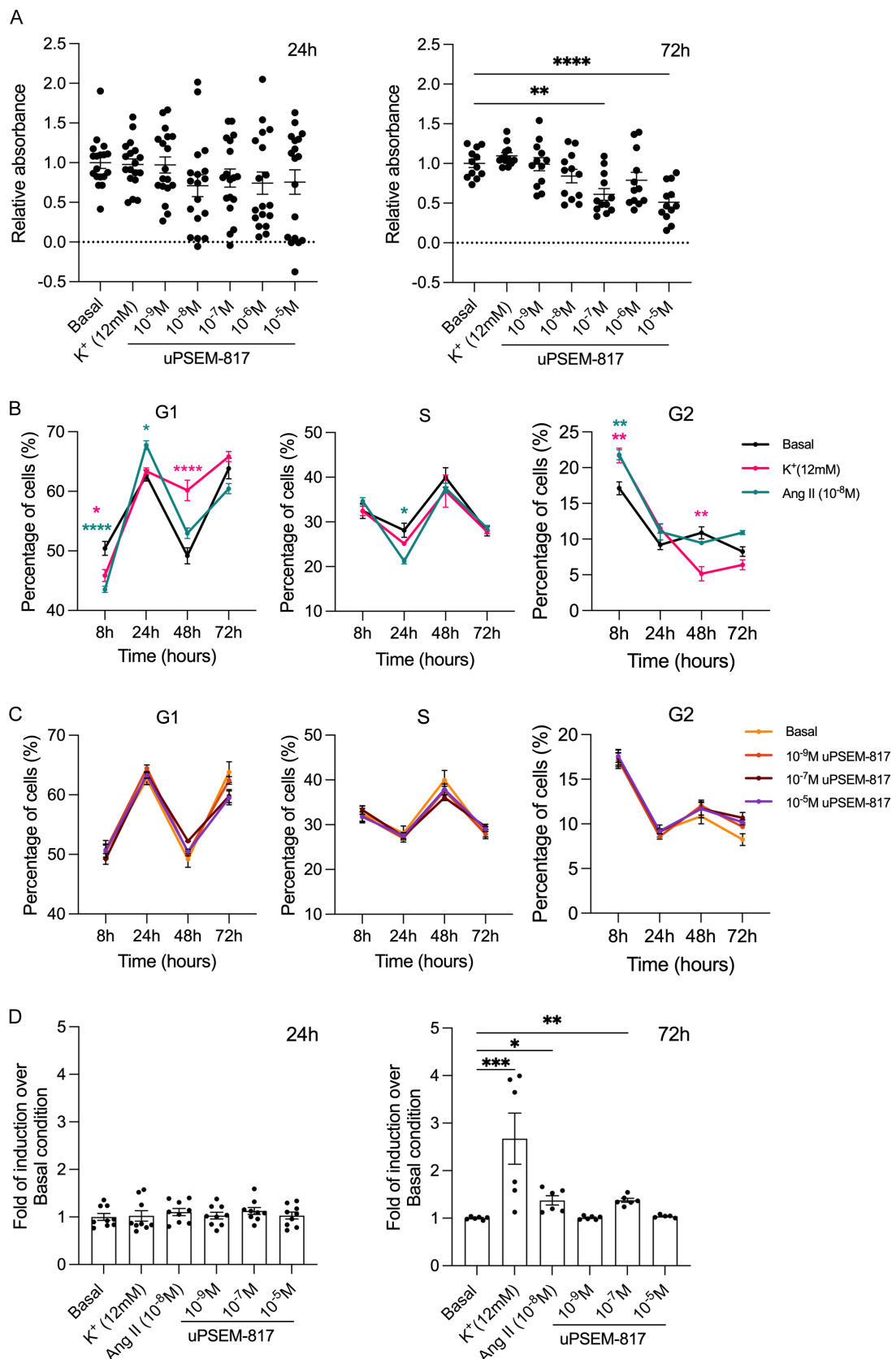


Figure 4. Effect of uPSEM-817 on cell proliferation and apoptosis. (A) Cell viability was measured on cells treated for 24h or 72h with 12mM K^+ or uPSEM-817 by MTS assay (Clone 17). (B) Cell cycle distribution measured by FACS using propidium iodide in response to $10^{-8}M$ AngII and 12mM K^+ (upper panel) and 10^{-9} , 10^{-7} and $10^{-5}M$ uPSEM-817 (lower panel).

(Clone 17). (C) Apoptosis determined by the proportion of cells in sub-G1 phase (Clone 17). (D-E) Proportion of cells in the sub-G1 phase after 24h (D) or 72h (E) in response to 12mM K⁺, 10⁻⁸M AngII and 10⁻⁹, 10⁻⁷ and 10⁻⁵M uPSEM-817. n=6 (cell cycle), n=12 (proliferation), P values were determined by one-way ANOVA followed by Bonferroni post-hoc comparisons tests, *, p<0.05; **, p<0.01; ****, p<0.0001

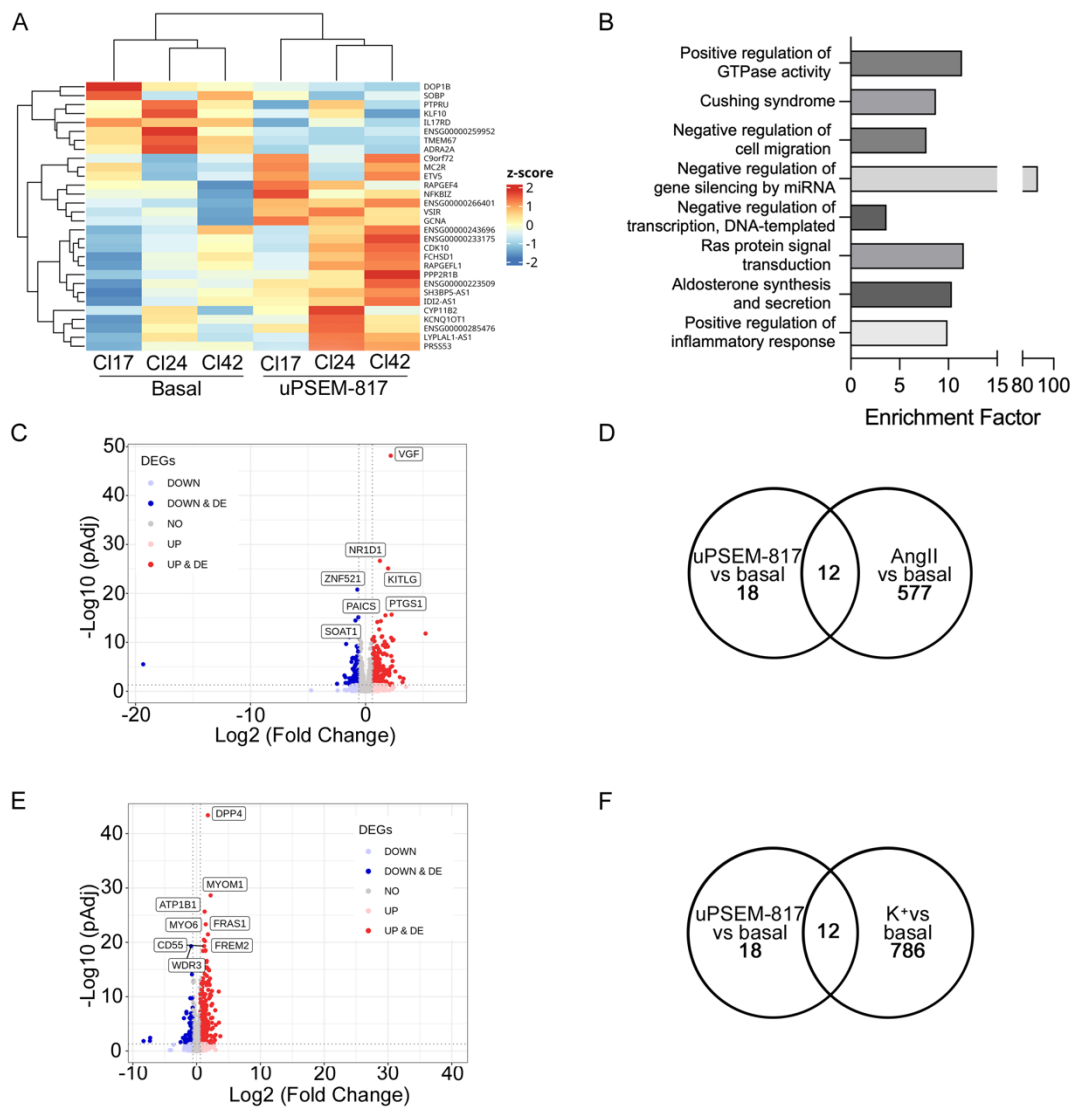


Figure 5. Gene expression profiles of H295R-S2 α 7-5HT3-R cells treated 24h with 10^{-7} M uPSEM-817, 10^{-8} M AngII or 12mM K⁺. (A) Hierarchical clustering of samples using the 28 differentially expressed genes in cells treated or not with 10^{-7} M uPSEM-817. (B) Biological process enrichments determined using the list of differentially expressed genes in cells treated or not with 10^{-7} M uPSEM-817. (C) Volcano plot showing the 4932 differentially in response to 10^{-8} M AngII. Differential expressed genes are highlighted as blue (down-regulated) or red (up-regulated) dots. (D) Venn diagram representing the common and different genes differentially expressed in response to 10^{-8} M AngII and 10^{-7} M uPSEM-817. (E) Volcano plot showing the 728 differentially in response to 12mM K⁺. The x-axis is the Log2 fold change between the two conditions; the adjusted p value based on $-\log_{10}$ is reported on the y-axis. Genes significantly different are highlighted as blue (down-regulated in cells treated with 12mM K⁺) or red (up-regulated in cells treated with 12mM K⁺) dots. (F) Venn diagram representing the common and different genes differentially expressed in response to 12mM K⁺ and 10^{-7} M uPSEM-817.